Measurement of (n, p) Reaction Cross Sections for Short-lived products ($T_{1/2}$=0.6~13.8 s) by 14 MeV Neutrons

Yoshimi Kasugai*[1], Yujiro Ikeda[1] and Hiroshi Takeuchi[2]
[1] *Center for Neutron Science, Japan Atomic Energy Research Institute*
Tokai-mura, Naka-gun, Ibaraki-ken 319-1195, Japan
[2] *Department of Fusion Engineering, Japan Atomic Energy Research Institute*
Tokai-mura, Naka-gun, Ibaraki-ken 319-1195, Japan
e-mail: kasugai@fnshp.tokai.jaeri.go.jp

Activation cross sections of the (n, p) reactions at 14 MeV for short-lived products were measured by using the D-T neutron source, FNS (Fusion Neutronics Source) at JAERI. Measured reactions were ^{11}B(n, p)^{11}Be ($T_{1/2}$=13.8 s), ^{18}O(n, p)^{18}N (0.63 S), ^{26}Mg(n, p)^{26}Na (1.07 s), ^{30}Si(n, p)^{30}Al(3.60 s) and ^{34}S(n, p)^{34}S (12.4 s). Using the present results, systematic trend of the (n, p) reaction cross sections for light-mass-targets was discussed.

1. Introduction

The cross sections for 14 MeV neutrons were fundamental data for fusion reactor design. Especially for light-mass-targets (A<40), reactions with charged particle emission, including (n, p), (n, α), etc. are relatively important in the viewpoint of activation, because the cross sections of charger particle emission reactions are much larger than those of the (n, 2n) reactions. However, accuracy of some experimental data for the light-mass-target has been insufficient because it is difficult to measure short-lived activities associated with the reactions.

Therefore we measured cross sections of five (n, p) reactions for the target nuclei with A=11~34. The half-lives of the products are ranged from 0.63 s to 12.4 s. The measured reactions and decay data of the products are listed in Table 1. In this report, the experimental procedure and measurement results are presented. Applicability of a systematic trend of the (n, p) reaction cross sections [1] for the light-mass-target is also discussed.

2. Experiment

D-T neutrons were produced via the ^{3}T(d,n)^{4}He reaction by bombarding a tritium-target with d^+ beams using the FNS facility. The d^+ beam current and energy were 2 mA and 350 keV, respectively. A semi-automatic sample transfer system, which rapidly transports a sample from the neutron field to a measurement position in front of the gamma-ray detector by compressed nitrogen air, were used for the measurement. Gamma-rays from the samples were measured with a Ge detector. The acquisition of a gamma-ray spectrum started when the sample reached a measurement position in front of the Ge detector. A schematic drawing of the sample transfer system is shown in Fig. 1. The procedure of the sample-transfer, irradiation, transfer and gamma-ray measurement were repeated 20~160 times for each sample.

The neutron energy, which are determined on the basis of the neutron spectra calculated by a Monte Carlo, were validated by measuring the ratio between ^{92}Nb(n, 2n)^{92m}Nb and ^{90}Zr(n, 2n)^{89m}Zr reaction rates. The uncertainty in the reaction energy determination was estimated to be less than 0.1 MeV.

The cross sections were derived by dividing reaction rates by neutron fluxes. The reaction rates were derived from the gamma-ray spectrum obtained by summing all the acquired spectra. The summed gamma-ray spectrum of a silicon sample is shown in Fig. 2. The neutron flux for each irradiation was obtained with the associated-α-particle counts monitored using the Multi-Channel Scaling (MCS) method.

The dwell time of the MCS was 1 s. In order to convert the α-particle counts to the neutron fluxes, the conversion factor was measured using the $^{27}Al(n,p)^{27}Mg$ reaction cross section.

The sources of errors were attributed to the neutron flux determination and the activation rate determination. The errors of the neutron flux determination came from the neutron yield determination using the associated-α-particle counting method and the conversion factor from the neutron yield to the neutron flux. The error of the standard cross section of the $^{27}Al(n,p)^{27}Mg$ reaction gave a main contribution to the error of the conversion factor. The errors of the reaction rate determination included the followings: gamma-ray counting statistics, a gamma-ray detection efficiency, half-lives and intensities of the products, sample weight. The final uncertainty was derived by adding the uncertainties of all the experimental parameters in a quadrate.

3. Results and Discussion

The measured cross sections are shown in Figs. 3.1 to 3.5, along with corresponding values from the literature and results from the comprehensive evaluation: JENDL-3 and ENDF/B-VI. Numerical values for the measured cross sections are given in Table 2 along with the experimental data.

For the $^{11}B(n, p)^{11}Be$ reaction, the JENDL-3 evaluation is more consistent with the present data than the ENDF/B-VI evaluation. The cross section for the $^{18}O(n, p)^{18}N$ reactions has not been measured previously. This work provided the first experimental data for the reaction. The JENDL-3 evaluation of $^{26}Mg(n, p)^{26}Na$ is higher by 10-20% than the present data. For the $^{30}Si(n, p)^{30}Al$ reactions, the ENDF/B-VI evaluation is consistent with the present data within the uncertainty. The JENDL-3 evaluation is lower by 50% than the present data. The cross section of the $^{34}S(n, p)^{34}P$ reaction were measured at the neutron energies between 13.4 and 14.9 MeV. The present data show the increasing trend of the excitation function around 14 MeV. The JENDL-3 evaluation is consistent with the present data.

Previously, using the cross section data measured at FNS [2, 3], the systematic trends of (n, p) reaction cross section were proposed [1]. In Fig. 4, the (n, p) cross sections divided by N-Z+1 are plotted as a function of (N-Z+1)/A, where N, Z and A are the mass, neutron and proton number of target nuclei, respectively. It has already been shown that the empirical rule shown in the figure is applicable for the target with A=19~188. In order to confirm the applicability of the empirical rule for the light mass target, the present data were plotted in the figure. The cross section data for $^{16}O(n, p)^{16}N$, $^{17}O(n, p)^{17}N$ reactions, which are previously measured [4], were also plotted in the figure. Except the $^{11}B(n, p)^{11}Be$ reactions, the present data also follow the empirical rule. This means that the empirical rule is applicable for the target with A≥16.

4. Conclusion

Activation cross sections for $^{11}B(n, p)^{11}Be$, $^{18}O(n, p)^{18}N$, $^{26}Mg(n, p)^{26}Na$, $^{30}Si(n, p)^{30}Al$ and $^{34}S(n, p)^{34}S$ reactions at 14 MeV were measured. The cross sections for the $^{18}O(n, p)^{18}N$ reactions were measured for the first time. Using the present results, it was shown that the simple empirical rule of the (n, p) reaction cross section at 14.9 MeV is applicable for the target with A≥16.

Acknowledgements

We would like to thank to FNS accelerator operation team, C. Kutukake, S. Tanaka, Y. Abe, Y. Seki and Y. Oginuma for their operation of FNS.

Reference

[1] Y. Kasugai et al., "Systematics for (n, p) Excitation Functions in the Neutron Energy between 13.3 and 15.0 MeV", Ann. Nucl. Energy, 23, 1429 (1996).

[2] Y. Ikeda et al., "Activation Cross Section Measurements for Fusion Structural Materials at Neutron

Energy from 13.3 to 15.0 MeV Using FNS Facility", JAERI-1312, (1988).
[3] C. Konno et al., "Activation Cross Section Measurements for at Neutron Energy from 13.3 to 15.0 MeV Using the FNS Facility", JAERI-1329, (1993).
[4] Y. Kasugai et al., "Cross-section Measurement for the $^{17}O(n, p)^{17}N$ Reaction by 14-MeV Neutrons", Nucl. Sci. Eng., 136, 258 (2000).

Table 1 Measured reaction and decay data [a]

Reaction	$T_{1/2}$ [b]	Eγ[keV] [c]	Iγ[%] [d]
$^{11}B(n, p)^{11}Be$	13.8 s	2124.5	35.5±1.8
$^{18}O(n, p)^{18}N$	0.63 s	821	44.5±1.8
$^{26}Mg(n, p)^{26}Na$	1.07 s	1808.6	99.0± 0.4
$^{30}Si(n, p)^{30}Al$	3.60 s	2235.2	65±1
$^{34}S(n, p)^{34}P$	12.4 s	2127.5	15± 2

[a] *Table of Isotopes*, 8th edition, R. B. Firestone and V.S. Shirley, editors, John Wiley & Sons, Inc. (1996).
[b] Half-life of the product.
[c] Energy of a gamma-ray with decay of a product.
[d] Gamma-ray intensity per decay.

Table 2 Numerical values of measured cross sections

Reaction	E_n[MeV] [a]	σ[mb] [b]
$^{11}B(n, p)^{11}Be$	14.94	5.2± 0.4
$^{18}O(n, p)^{18}N$	14.94	1.15±17
$^{26}Mg(n, p)^{26}Na$	14.94	31±4
$^{30}Si(n, p)^{30}Al$	14.94	34±5

[a] Neutron energy.
[b] Measured cross section value.

Reaction	E_n[MeV]	σ[mb]
$^{34}S(n, p)^{34}P$	14.94	100±22
	14.68	88±19
	14.37	88±20
	14.02	90±20
	13.68	82±20
	13.36	88±22

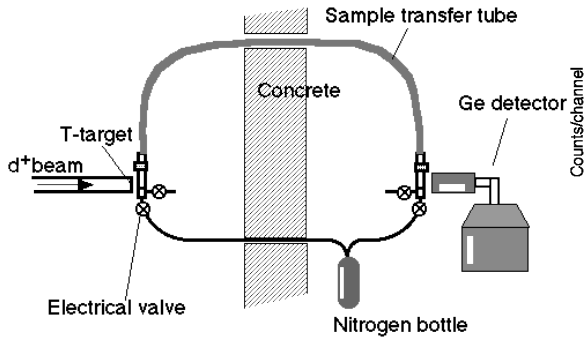

Fig. 1 Schematic drawing of the sample transfer system

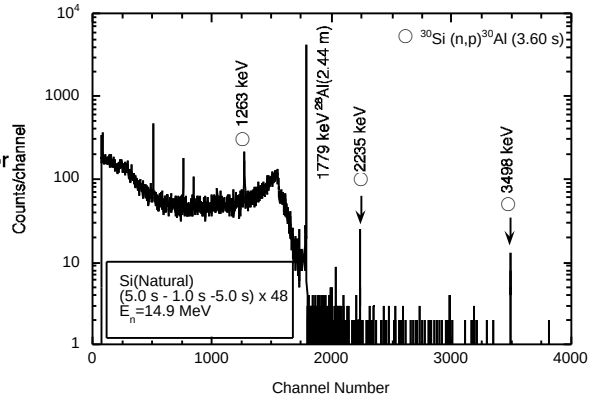

Fig.2 Gamma-ray spectrum of the silicon sample.

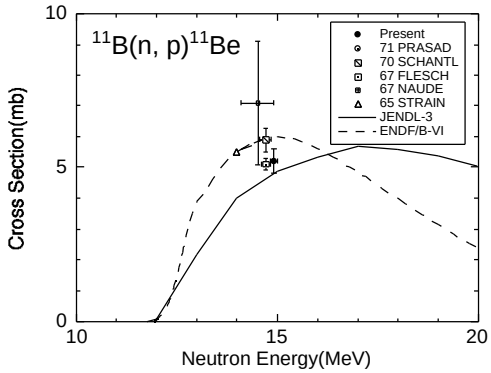

Fig. 3.1 Cross section of the ^{11}B(n, p)^{11}Be reaction

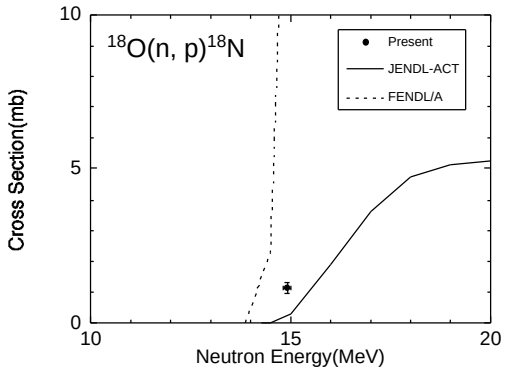

Fig. 3.2 Cross section of the ^{18}O(n, p)^{18}N reaction.

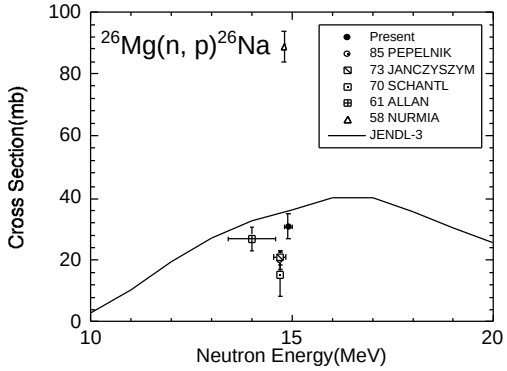

Fig. 3.3 Cross section of the ^{26}Mg(n, p)^{26}Na reaction

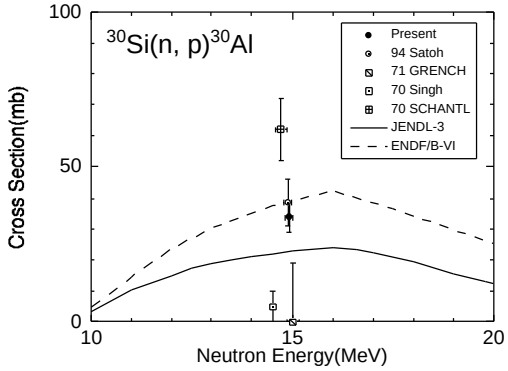

Fig. 3.4 Cross section of the ^{30}Si(n, p)^{30}Al reaction

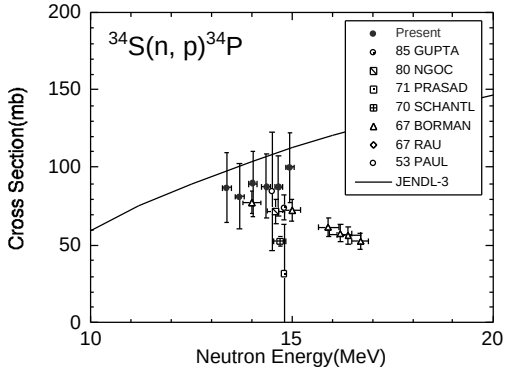

Fig. 3.5 Cross section of the ^{34}S(n, p)^{34}P reaction

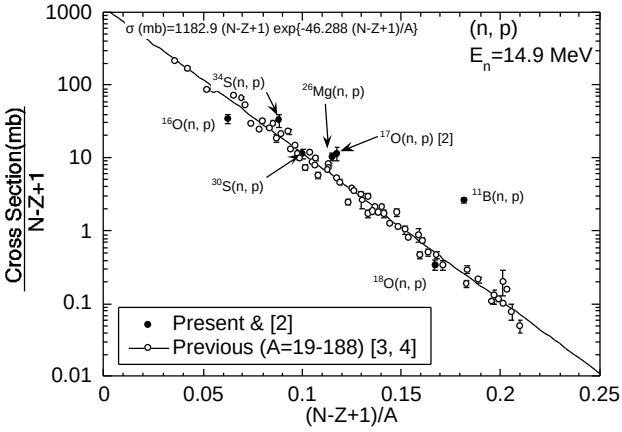

Fig. 4 Systematics of the (n, p) reaction cross sections